

Effect of Lip/Nozzle Deflection Angle on the Aerodynamic and Propulsive Characteristics of Propulsion Wing Unit

Minghao LI[1,2], Zhou Zhou[1,2], Kelei WANG[1,2]

[1]School of Aeronautics, Northwestern Polytechnical University, Xi'an 710072, China
[2]National Key Laboratory of Air, Northwestern Polytechnical University, Xi'an 710072, China

Abstract

To address the challenge of balancing hovering and cruising efficiency for electric vertical takeoff and landing (eVTOL) unmanned aerial vehicles (UAVs), this paper conducts numerical simulation and mechanism study on a distributed propulsion wing unit with variable lip/nozzle angles. A parametric model describing the deflected configuration is established based on the super-ellipse equation, fourth-order Bézier curve, and CST method. Using the MRF approach, the flow characteristics are systematically simulated within a freestream velocity range of 0–30 m/s, covering deflection angles from –40° to +40° under different rotational speeds. The results show that the deflection angle significantly affects both aerodynamic and propulsive performance of the distributed propulsion wing unit. A single deflection scheme exhibits pronounced adaptability to specific operating conditions, while a coupled deflection scheme can achieve performance breakthroughs under appropriate combinations. Moreover, different configurations show distinct performance characteristics across various speed ranges. From the perspective of aerodynamic-propulsive coupling, this study provides a theoretical basis and practical solution for the integrated design of distributed propulsion wing units capable of efficient operation in both hover and cruise conditions.

Keywords: eVTOL UAV; Distributed Propulsion Wing; Parametric Model; Aerodynamic-Propulsive Coupling; Efficient Integrated Design

1. Introduction

Facing the demand for high efficiency, low noise, and low emission "green aviation" driven by the low-altitude economy, electric vertical takeoff and landing (eVTOL) unmanned aerial vehicles (UAVs) have shown great potential [1]. However, efficiency remains an eternal pursuit in aircraft design. From lift-and-thrust compound configurations to tilt-rotor/tilt-wing designs, and further to induced deflection concepts, from rotor-based propulsion to ducted fan systems, and from centralized propulsion to distributed propulsion, researchers have never ceased exploring ways to improve efficiency [2]. Currently, even though a ducted fan system can achieve a wide operating speed range after careful design, any power unit with a fixed external shape inevitably has only one optimal operating condition. Consequently, a shape optimized for that condition cannot simultaneously meet the requirements for efficient hover and efficient cruise. To maximize hovering efficiency, the duct needs to generate as large a flow rate as possible, which inevitably requires large expansion angles for both the lip and the nozzle. In contrast, during cruise, the expansion angles of the duct lip and nozzle should be as small as possible to reduce drag and improve propulsive efficiency [3].

To address the fundamental contradiction mentioned above, researchers have carried out a series of studies from the perspective of deformable ducts, actively or passively adjusting key geometric parameters of the duct to achieve high efficiency under both hovering and cruising conditions. Xiang [4] proposed a duct with variable lip and diffuser angles, using flexible duct wall material and continuously adjusting the lip radius driven by an actuator to improve flow separation and enhance efficiency. Although this design has limited deformation capacity and thus cannot reach the theoretical optimum under arbitrary inflow conditions, its adaptability to multiple operating conditions is significantly better than that of conventional fixed-geometry ducts. In 2021, Xagon Solutions in the

https://doi.org/10.71945/icas2026_0200

United States developed the Adaptive Ducted Fan [5], in which inlet flaps are installed at the lip. Each segmented flap autonomously adjusts its deflection angle based on local air pressure, enabling passive continuous deformation of the lip and effectively improving efficiency over the entire operating range. Liu YT [6] approached the problem from the perspective of outlet deformation and proposed a variable outlet ducted system: during vertical takeoff and landing, the outlet expands to reduce downwash velocity, thereby reducing duct size and weight for a given efficiency; during cruise, the outlet contracts to reduce frontal area, decrease forward flight drag, and improve propulsive efficiency. Lilium, for its wing-mounted distributed ducted fan aircraft, installed Variable Area Nozzles at the duct outlet [7]. By changing the effective outlet area, the fan operating point is shifted to high-efficiency regions unreachable with fixed-geometry designs, thereby meeting the high-efficiency demands of both hover and cruise simultaneously, providing a new approach for ducted fan design. In summary, varying the deflection angles of the duct lip and nozzle is an effective way to alleviate the "two-point contradiction" between hover and cruise. However, existing studies are mostly application-oriented and have not yet formed a systematic description of the propulsion-aerodynamic coupling characteristics and flow mechanisms of ducted fans (especially special configurations such as the distributed propulsion wing unit [8]) under varying geometric parameters.

This paper takes the distributed propulsion wing unit, similar to that of the Lilium Jet, as the research object. First, a parametric modeling method for the ducted fan with deflectable lip and nozzle is developed to achieve programmatic automatic generation of complex curved surfaces. Then, based on computational fluid dynamics methods, numerical simulations are carried out using commercial software FLUENT. By investigating the influence mechanism of lip and nozzle deflection angles on the efficiency of the distributed propulsion wing unit under different velocities and rotational speeds, the aerodynamic/propulsive coupling characteristics and physical mechanisms under varying key geometric parameters are revealed. This study provides theoretical basis and reference for alleviating the contradiction between hovering and cruising efficiency of eVTOL UAVs.

2. Research object and method

2.1 Geometry model

The Distributed Propulsion Wing (DPW) layout breaks the traditional concept of airframe-engine integration. Compared with conventional distributed circular ducted fans, it truly achieves complete integration of the ducted propulsion system with the aerodynamic surface of the wing, where internal and external flows are fully mixed—the wing is the propulsion, and the propulsion is the wing. According to the study by Wang et al. [9] on the propulsive characteristics of the Distributed Propulsion Wing, it is found that the DPW exhibits significant unit characteristics. Therefore, this paper starts from the propulsion wing unit and conducts research on lip/nozzle deformation.

The baseline propulsion wing unit has an aspect ratio of $AR = D/c = 1$, where c is the duct chord length and D is the inner wall diameter, which is 250 mm. Considering manufacturing tolerances, the tip clearance is maintained at 0.4% of the propeller radius. As shown in the figure below, the propulsion wing unit can be divided according to a "square-circle-square" layout. The core of the unit includes the rotor, hub, cylindrical duct section, the "square-circle" inlet, and the "circle-square" outlet. The outer wall adopts conventional upper and lower wing surfaces as the duct-wing. During the study, the geometric models of the rotor, hub, and cylindrical duct section are kept fixed, while parametric modeling is performed on the "square-circle" inlet, the "circle-square" outlet, and the duct-wing surface to achieve deflection of the lip and nozzle sections.

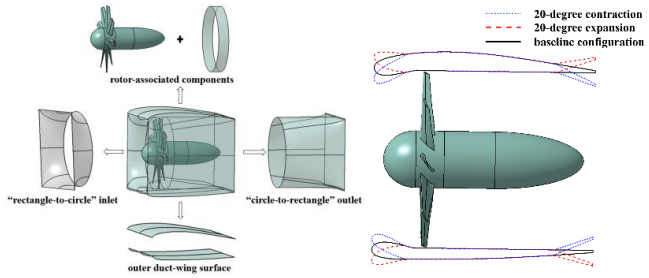


Figure 1 – Schematic of the Propulsive Wing Unit: Disassembly and Lip/Nozzle Deflection.

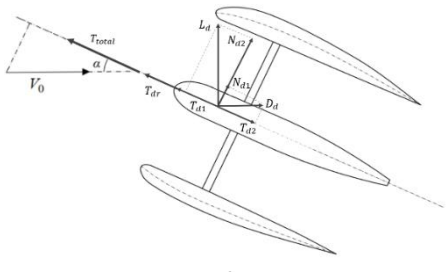


Figure 2 – Force definition.

For the research object in this paper, when considered as an aerodynamic component, the ducted fan can be equivalent to an airfoil-like structure, and its aerodynamic characteristics are defined in a manner consistent with conventional wings. The forces are decomposed into lift and drag components along the wind axis system. This paper focuses on the aerodynamic performance of the duct wall as an aerodynamic surface under internal-external flow coupling. Therefore, the term "aerodynamic characteristics" here specifically refers to the lift (L_d) and drag (D_d) generated by the duct wall. When considered as a propulsive component, the forces are decomposed into thrust and normal force along the duct axis direction, which is consistent with the conventional body axis system. In this case, in addition to the duct wall thrust (T_d), the rotor thrust component (T_r) must also be superposed. The conversion equations between aerodynamic and propulsive force can be derived as follow:

$$T_{total} = T_d + T_r \tag{1}$$

$$T_d = T_{d1} + T_{d2} = L_d \times \sin(\propto) - D_d \times \cos(\propto) \tag{2}$$

$$N_d = N_{d1} + N_{d2} = L_d \times cos(\propto) + D_d \times sin(\propto) \tag{3}$$

2.2 Geometry model

To address the internal external flow coupling problem of the propulsion wing unit [10], this paper adopts the commercial software FLUENT and solves the Reynolds Averaged Navier Stokes (RANS) equations using the coupled k ω Shear Stress Transport (SST) turbulence model [11]. This numerical simulation method is widely used in engineering applications and offers good robustness. In the computation, spatial discretization is performed using the Roe scheme with second order upwind MUSCL (Monotone Upstream Centered Scheme for Conservation Laws) interpolation, while temporal discretization and advancement are carried out using the implicit AF (Approximate Factorization) method. Pressure far field boundary conditions are applied.

Furthermore, to meet the requirement for refined flow field analysis of the internal-external flow coupling of the propulsion wing unit [12], this paper adopts a structured grid patching method based on the real blade model to couple the rotational domain and the far-field stationary domain (the rotational domain is the inner flow region near the blades, while the remaining region is the far-field domain, as shown in Figure 3). The quasi-steady solution is obtained using the Multiple Reference Frame [13] (MRF) method, which is widely used in aerodynamic calculations for rotating bodies with a fixed axis.

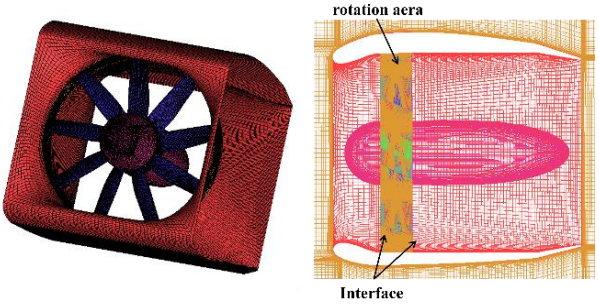


Figure 3 – Schematic of the Ducted Fan Computational Grid.

Furthermore, to balance computational efficiency and accuracy while avoiding misjudgment of ducted fan performance due to numerical errors, three computational grid models with different mesh densities are established. A grid independence study is conducted under the conditions of altitude $H = 69m$, freestream velocity $V = 30m/s$, rotational speed $N = 9000r/min$, and angle of attack $\alpha = 0°$. The first-layer grid height is set to $d = 1.25 \times 10^{-5}m$ for all grids, ensuring $y^+ = 1$. The main differences among the three grids lie in the refinement scales at the duct leading and trailing edges, as well as the mesh density on the rotor surface.

All computations are performed on the same server equipped with 64 cores, 128 threads, and 256 GB of RAM. The computational results for the three grids are presented in Table 1. Using the finest grid as the benchmark, the errors of the medium-density grid are all within 1%, while the number of grid cells is reduced by half, significantly shortening the computational time and improving efficiency. Therefore, considering both computational accuracy and efficiency, the subsequent numerical simulations of the ducted fan will mainly adopt the configuration with 2.58 million grid cells.

Table 1 – Comparison of mesh information and simulation results using different meshes.

Parameter	Coarse mesh	Medium mesh	Fine mesh
Leading/Trailing edge refinement size(mm)	0.5	0.3	0.1
Duct wall mesh size(mm)	0.8	0.5	0.2
Rotor surface mesh size(mm)	0.8	0.5	0.2
Total grid count	1097000	2586000	6926000
Total lift(N)	7.6441	8.0608	8.0925
Total thrust(N)	0.9345	1.1429	1.1467
Rotor thrust(N)	3.1503	3.1705	3.1768
Power(W)	687.0363	689.3523	690.6275
Computing time(h)	1.5	3.5	7.5

2.3 Experimental facilities

To validate the computational method, ground tests are conducted in the FD-1200 low-speed propeller wind tunnel using an open test section measuring 1.2 m (width) × 1.2 m (height) × 3 m (length), with a velocity range of 0~85 m/s, turbulence intensity < 0.2%, velocity uniformity < 0.5%, flow angularity < 0.5%, axial static pressure gradient < 0.5%, and velocity stability < 0.5%. The propulsion and aerodynamic performance of the propulsion wing unit are measured. The outer duct wall is manufactured using photopolymer resin via 3D printing, and the rotor section is made of carbon fiber composite to ensure geometric accuracy and maintain negligible deformation throughout the experiment. An ATI six-component balance and pressure scanners are used to measure force characteristics and pressure distribution, respectively. The test conditions include freestream velocities $V = 0\sim30m/s$ at intervals of $\Delta V = 30m/s$, and rotational speeds $N = 3000\sim11000r/min$.

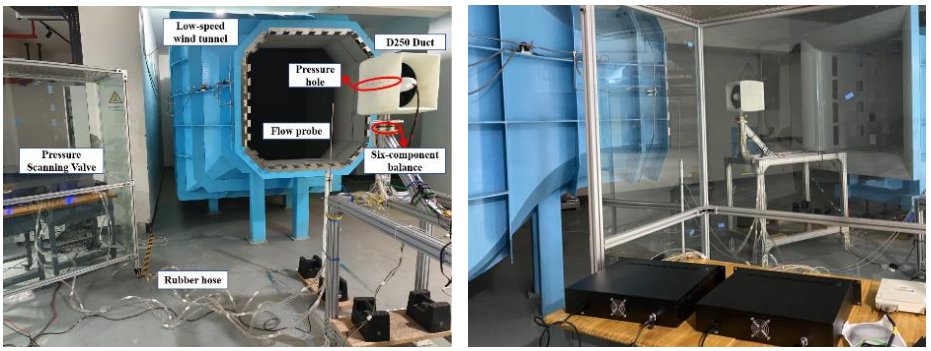
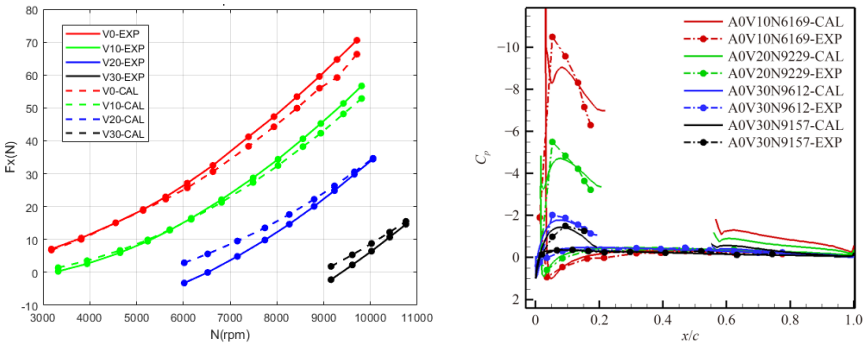


Figure 4 – Schematic of the Wind Tunnel Test Setup for the DPW Unit.

Figure 5 presents a comparison between experimental and computational results, where “EXP” denotes wind tunnel results and “CAL” denotes computational results. Under zero freestream velocity,

maximum error between numerical and experimental results is within 5%. As freestream velocity increases, thrust of the propulsion wing unit decreases significantly, leading to a large error between MRF numerical results and experimental values near starting rotational speed. However, as rotational speed increases, error continuously decreases. Overall, the slopes of the propulsive characteristic curves and their trends with rotational speed remain consistent between both approaches. Furthermore, under different velocity and rotational speed conditions, computed wall pressure distributions are in agreement with experimental results. This indicates that, for the present object, the MRF method can capture the actual aerodynamic and propulsive characteristics.



(a)Thrust (b) Pressure distribution

Figure 5 – Comparison of CFD and Wind Tunnel Test Results.

3. Parametric Modeling of the DPW Unit

As described in Section 2.1, this paper establishes parametric models for three parts of the propulsion wing. For the airfoil profile of the outer wall, the CST parameterization method [14] is adopted. For the inner curved surfaces of the ducted fan, namely the "square-to-circle" inlet and the "circle-to-square" exhaust duct, the cross-sectional profiles along the streamwise direction are parameterized using the super-ellipse equation[14]. Meanwhile, the ridge lines $a(t)$, $b(t)$, and $m(t)$ of the upper and lower "square-to-circle" inlet and "circle-to-square" exhaust duct are parameterized using fourth-order Bézier curves.

$$B(t) = (1-t)^4 P_0 + 4t(1-t)^3 P_1 + 6t^2(1-t)^2 P_2 + 4t^3(1-t)P_3 + t^4 P_4 \,, t \in [0,1] \tag{4}$$

$$(\frac{y}{b})^m + (\frac{z}{a})^m = 1 \tag{5}$$

In the equations: t is the control parameter ranging from 0 to 1, P_i are control point coordinates, y and z are coordinates of a point on the super-ellipse cross-section, a is the semi-major axis of the super-ellipse, b is the semi-minor axis of the super-ellipse, and m is the super-ellipse exponent. The specific method and baseline parameter settings can be found in Ref. [9] and are not repeated here. It should be noted that, based on the baseline configuration, this study introduces rotation points and rotation angle parameters for the lip and nozzle of the upper and lower walls, resulting in eight parameters in total. After generating the baseline propulsion wing unit, each $b(t)$ curve is rotated and updated according to these parameters, and then the $m(t)$ curves are recalculated, ultimately achieving automatic surface generation after lip/nozzle rotation (as shown in the figure below).

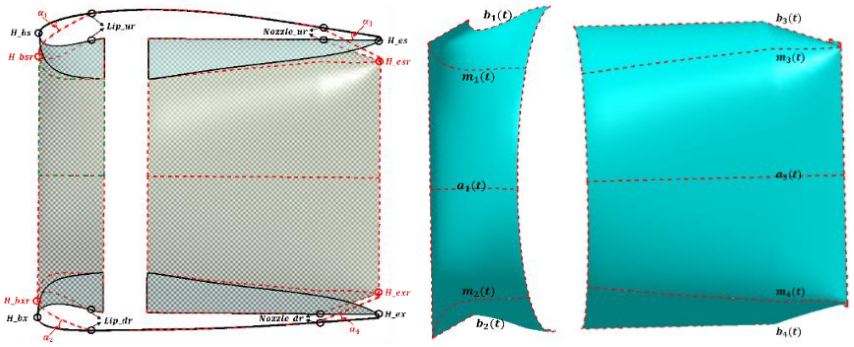


Figure 6 – Schematic of Additional Parameters and Control Curves.

To more cleanly investigate the effects of lip and nozzle diffusion and contraction on the propulsion/aerodynamic characteristics of the propulsion wing unit, this study keeps lip and nozzle streamwise coordinates unchanged during rotational deformation, ensuring only lip and nozzle areas are altered. Therefore, after generating the baseline configuration, the semi-major axis curve $a(t)$ remains unchanged, while only the semi-minor axis curve $b(t)$ and the shape control parameter curve $m(t)$ are modified. Taking the upper lip as an example, the update formula for $b(t)$ in the rotated section is given below. The $m(t)$ curve is obtained by inversely solving the super-ellipse equation (4), following the same approach as in Ref. [10].

$$dx = x_{current} - Lip_{_ur} \tag{6}$$

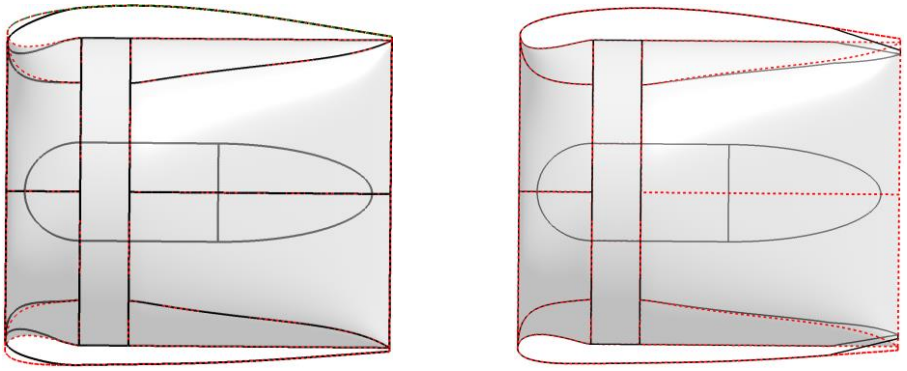
$$b(i) = b(i) + dxsin(a1) \tag{7}$$

Where $x_{current}$ is the local x-coordinate in the rotated section, and Lip_{ur} is the x-coordinate of the upper lip rotation point, $a1$ represents the deflection angle.

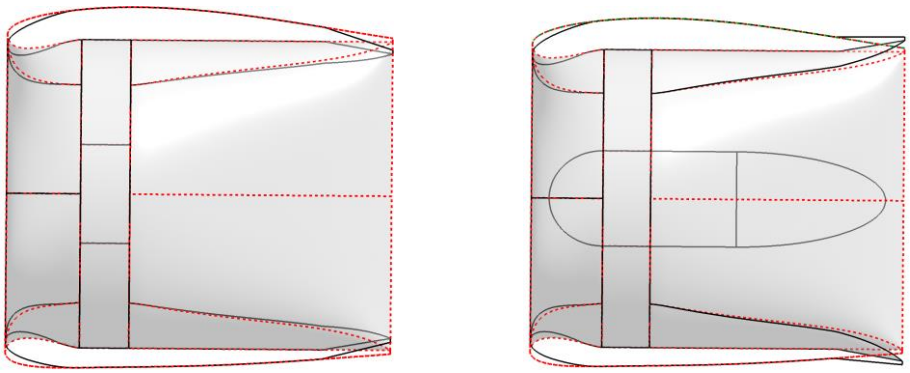
4. Performance of DPW Units with Different Lip/Nozzle Deflection Angles

4.1 Propulsion characteristics

Based on the parametric modeling method described in Section 3, numerical simulations are carried out using the MRF method for a series of propulsion wing unit configurations with different lip and nozzle deflection angles. Simulations are conducted at two freestream velocities, 0 m/s and 30 m/s, with rotational speeds ranging from 3000 to 10,000 r/min and deflection angles varying from –40°to +40° (negative angles indicate outward expansion deformation, positive angles indicate inward contraction deformation). Figure 7 shows a schematic of four deflection schemes, where “Only lip” denotes the configuration with only lip deflection, “Only nozzle” denotes the configuration with only nozzle deflection, “Synchronous” denotes the configuration with synchronous lip and nozzle deflection, and “Opposite” denotes the configuration with opposite deflection (namely lip expands while nozzle contracts; the figure is drawn according to the lip angle variation).

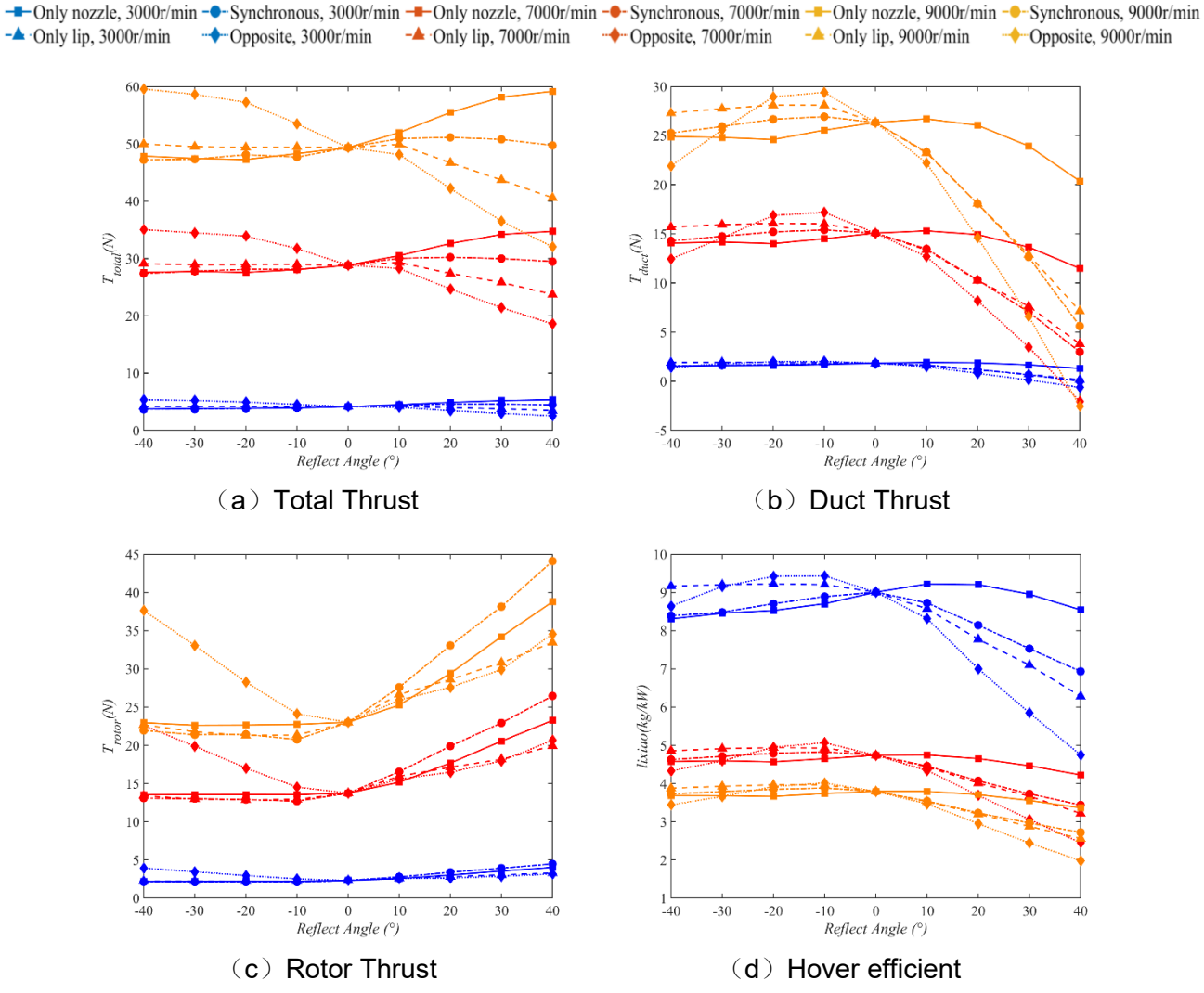


（a）Only lip　　（b）Only nozzle



（c）Synchronous　　（d）Opposite

Figure 7 – Geometric schematic of four different deformation schemes (red dashed line denotes the baseline configuration).



（a）Total Thrust　　（b）Duct Thrust

（c）Rotor Thrust　　（d）Hover efficient

Figure 8 – Propulsion characteristic curves of the propulsion wing unit at different deflection angles under hovering condition ($\alpha = 0°, V = 0m/s$).

Figure 8 presents the propulsion characteristic curves of the propulsion wing unit under hovering condition for the four deformation schemes. It can be observed that:

(1) Under hovering condition with zero freestream velocity, the total thrust of the “Only lip” configuration increases slightly with lip expansion angle, with overall thrust efficiency higher than the baseline, and the growth rate of total thrust slightly increases with rotational speed. The duct wall thrust exceeds the baseline across all expansion angles, but first increases and then decreases with expansion angle, while rotor thrust remains slightly below baseline, possibly due to weakened suction acceleration effect at excessive expansion angles. As lip contraction angle increases, duct wall thrust

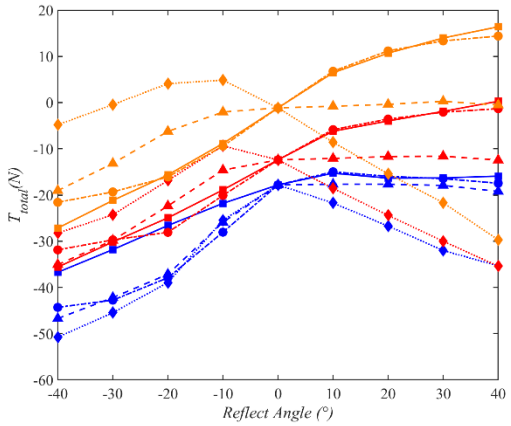
drops significantly, while rotor thrust rises noticeably. However, the rotor thrust increase is still less than the duct wall thrust decrease, causing a substantial drop in total thrust, with thrust efficiency far below baseline.

(2) For the “Only nozzle” configuration, with nozzle expansion, both total thrust and thrust efficiency are lower than the baseline, and the total thrust further decreases with rotational speed. The duct wall thrust remains below the baseline across all expansion angles, first decreasing and then increasing with expansion angle, possibly due to changes in wall pressure distribution and flow attachment caused by the jet. The rotor thrust shows a similar trend. With nozzle contraction, total thrust increases with contraction angle: duct wall thrust first rises then falls, while rotor thrust keeps increasing. This indicates that a contracting accelerating jet can increase thrust, but excessive contraction may cause choking or separation, reducing duct wall thrust. Under combined effects, thrust efficiency improves within a certain contraction angle range.

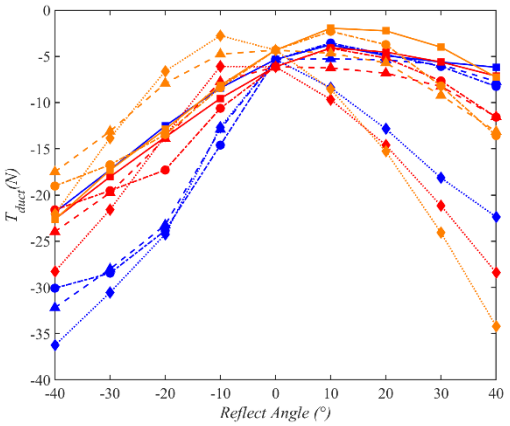
(3) For “Synchronous”, thrust characteristics are intermediate between the prior two. Duct wall thrust is closer to “Only lip”. Rotor thrust far exceeds single-deformation configurations in contraction range, and nearly coincides with “Only lip” in expansion range, indicating lip variation dominates propulsion characteristics at low speeds. Total thrust lies between the other two, with little change from baseline, but rotor thrust is slightly higher, yielding thrust efficiency always below baseline.

(4) For the “Opposite” configuration, the thrust characteristics better combine the advantages of “Only lip” and “Only nozzle”. When lip expansion and nozzle contraction occur simultaneously with deflection angles within ±20°, the thrust and efficiency of this configuration are significantly higher than those of the other three. However, as rotational speed increases, the efficiency gain diminishes, gradually approaching the single-deformation configurations, yet still remaining the highest overall. Moreover, when the deflection angle further increases or the configuration enters the state of lip contraction with nozzle expansion, the thrust characteristics become the lowest, indicating a distinct optimal operating range.

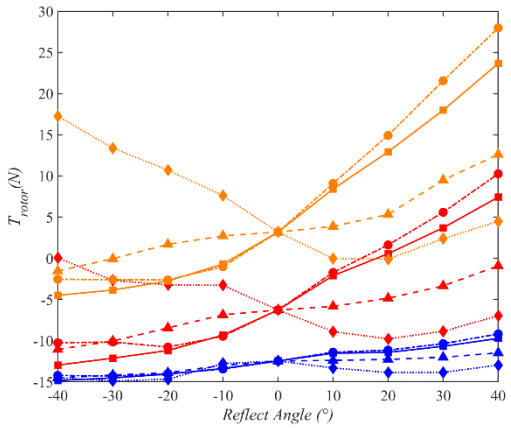




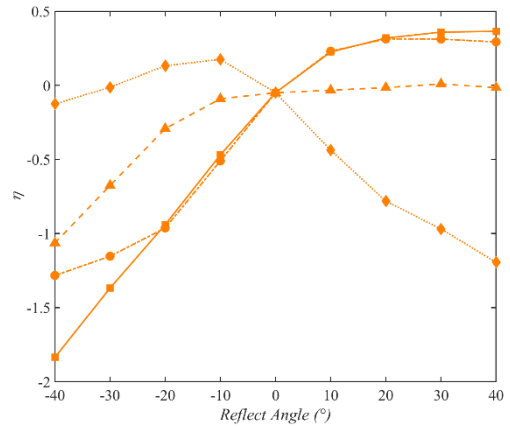
（a）Total Thrust



（b）Duct Thrust



（c）Rotor Thrust



（d）Cruise efficient

Figure 9 – Propulsion characteristic curves of the propulsion wing unit at different deflection angles under cruising condition ($\alpha = 0°, V = 30m/s$).

Figure 9 presents the propulsion characteristic curves of the propulsion wing unit under cruising condition for different deformation schemes. At low rotational speeds, the propulsion wing unit exhibits significant drag characteristics, making efficiency analysis meaningless. Therefore, the efficiency curves are only plotted for 9000 r/min. It can be observed that:

(1) At cruising speed, even when the rotational speed increases to 9000 r/min, the “Only lip” configuration fails to generate effective thrust. As the lip expansion angle increases, rotor thrust decreases on one hand, while on the other hand, the wetted area of the duct increases significantly in high-speed freestream, leading to increased duct wall drag and substantial loss of duct thrust, so the total thrust drops rapidly. When the lip contracts, similar to the hovering condition, duct thrust decreases while rotor thrust increases, and the total thrust remains nearly unchanged; only after the contraction angle reaches 40° does it slightly degrade, possibly due to flow separation near the lip caused by excessive contraction.

(2) The “Only nozzle” configuration exhibits thrust characteristics similar to “Only lip” when the nozzle expands, but with more severe performance degradation. As the expansion angle increases, both the duct wall aerodynamic drag and the rotor thrust loss are significantly larger than those of “Only lip” at the same angle, resulting in lower total thrust and efficiency. Notably, when the nozzle contracts, the thrust characteristics improve markedly: the trends of duct thrust and rotor thrust are consistent with those under hovering condition, and total thrust increases significantly with contraction angle. After the contraction angle exceeds 10°, its efficiency remains superior to all other configurations, demonstrating the best propulsive performance.

(3) Different from the hovering condition, at cruising speed, the propulsion characteristic curves of the “Synchronous” configuration nearly coincide with the “Only nozzle”, indicating that nozzle variation dominates the propulsion characteristics of this configuration under high-speed conditions, while the effect of lip deflection is very limited. This characteristic is consistent with the performance of “Only lip” at cruising speed.

(4) At cruising speed, the “Opposite” configuration also exhibits reasonably good propulsion characteristics. However, due to the inability of lip expansion to generate effective gain under high-speed conditions, its overall propulsive performance is inferior to that of “Only nozzle”. Moreover, when the absolute deflection angle exceeds 20°, both thrust and efficiency decrease, leading to degraded overall propulsive performance.

Overall, under hovering condition, the “Opposite” configuration exhibits a distinct advantage. Although its efficiency advantage gradually diminishes as rotational speed increases, it still surpasses all other configurations in thrust characteristics within a certain angle range. Meanwhile, single-deformation schemes (only lip or only nozzle) can also effectively improve propulsive performance. The “Only lip” configuration with lip expansion achieves higher thrust efficiency than the baseline at similar thrust and power levels. The “Only nozzle” configuration, within a nozzle contraction angle below 20°, maintains a significant increase in efficiency while operating at notably higher thrust and power than the baseline. On the other hand, under cruising condition, the “Only nozzle” configuration demonstrates the best propulsive performance when the nozzle contracts. Once the contraction angle exceeds 10°, its efficiency remains superior to all other configurations, making it the most advantageous deformation scheme for cruising. The “Only lip” configuration fails to generate effective thrust regardless of lip expansion or contraction; only under lip contraction can it barely keep the total thrust unchanged, resulting in poor overall propulsive performance. The characteristics of the “Synchronous” configuration are almost entirely dominated by nozzle variation, with lip deflection playing a negligible role, so its performance is essentially identical to that of “Only nozzle”. Although the “Opposite” configuration still achieves considerable propulsive performance, its overall capability is slightly inferior to that of “Only nozzle” due to the ineffectiveness of lip expansion at high speeds, and its performance degrades significantly at large deflection angles.

4.2 Aerodynamic characteristics

Note that the rotor and hub are typical power components and cannot generate effective aerodynamic characteristics. The duct wall (the structure excluding the rotor and hub) is the main aerodynamic component. Therefore, the aerodynamic characteristics of the propulsion wing are primarily embodied by the duct wall itself, and the aerodynamic analysis in this section specifically refers to the

aerodynamic forces generated by the duct wall. At low freestream velocities, the duct wall is dominated by thrust characteristics and hardly generates significant lift [15]. At higher freestream velocities, the lift characteristics of the baseline configuration are similar to those of a conventional wing, where external flow dominates [16] and rotational speed has a very weak influence on lift characteristics [17]. The aerodynamic forces generated by the duct wall differ from the duct thrust (T_d) in the body axis system discussed earlier and must be decomposed in the wind axis system to obtain lift (L_d) and drag (D_d). Based on this, the rotational speed is fixed at 7000 r/min in this section, and numerical simulations are carried out under a freestream velocity of 30 m/s.

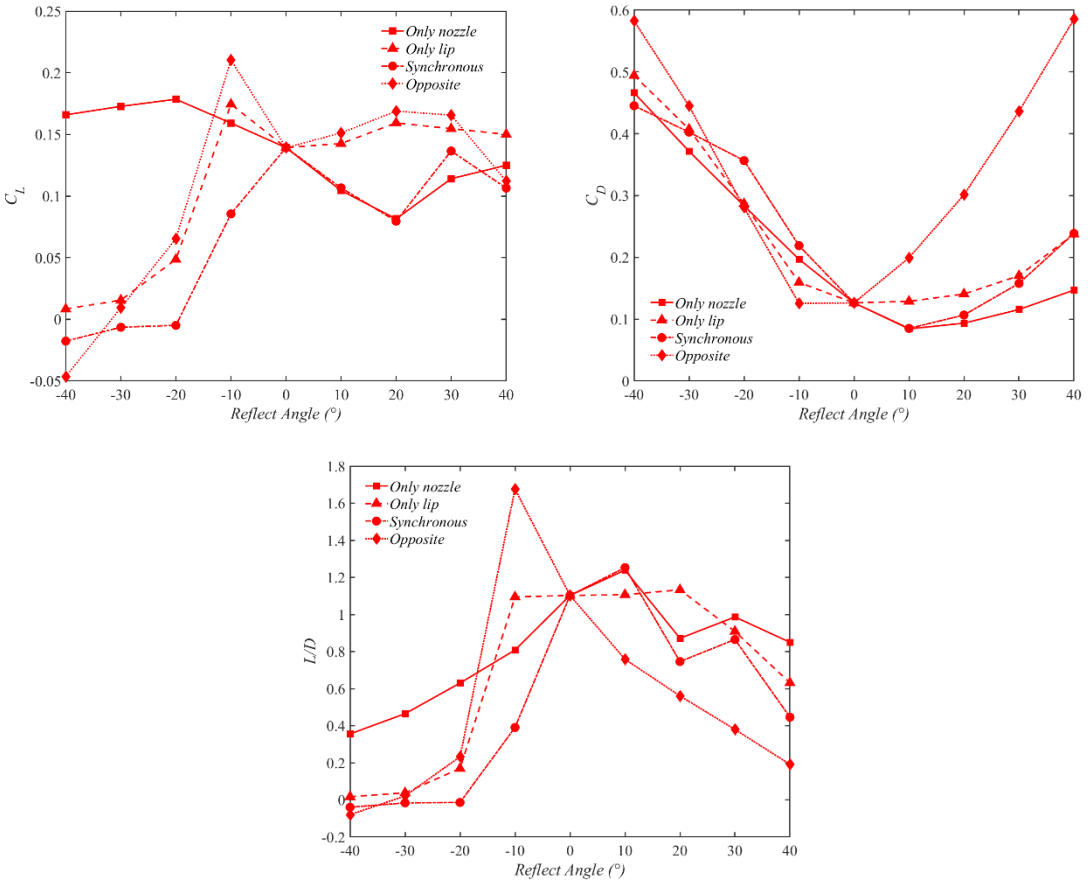


Figure 10 – Lift characteristic curves of various configurations versus deflection angle at zero angle of attack ($N = 7000r/min, V = 30m/s$).

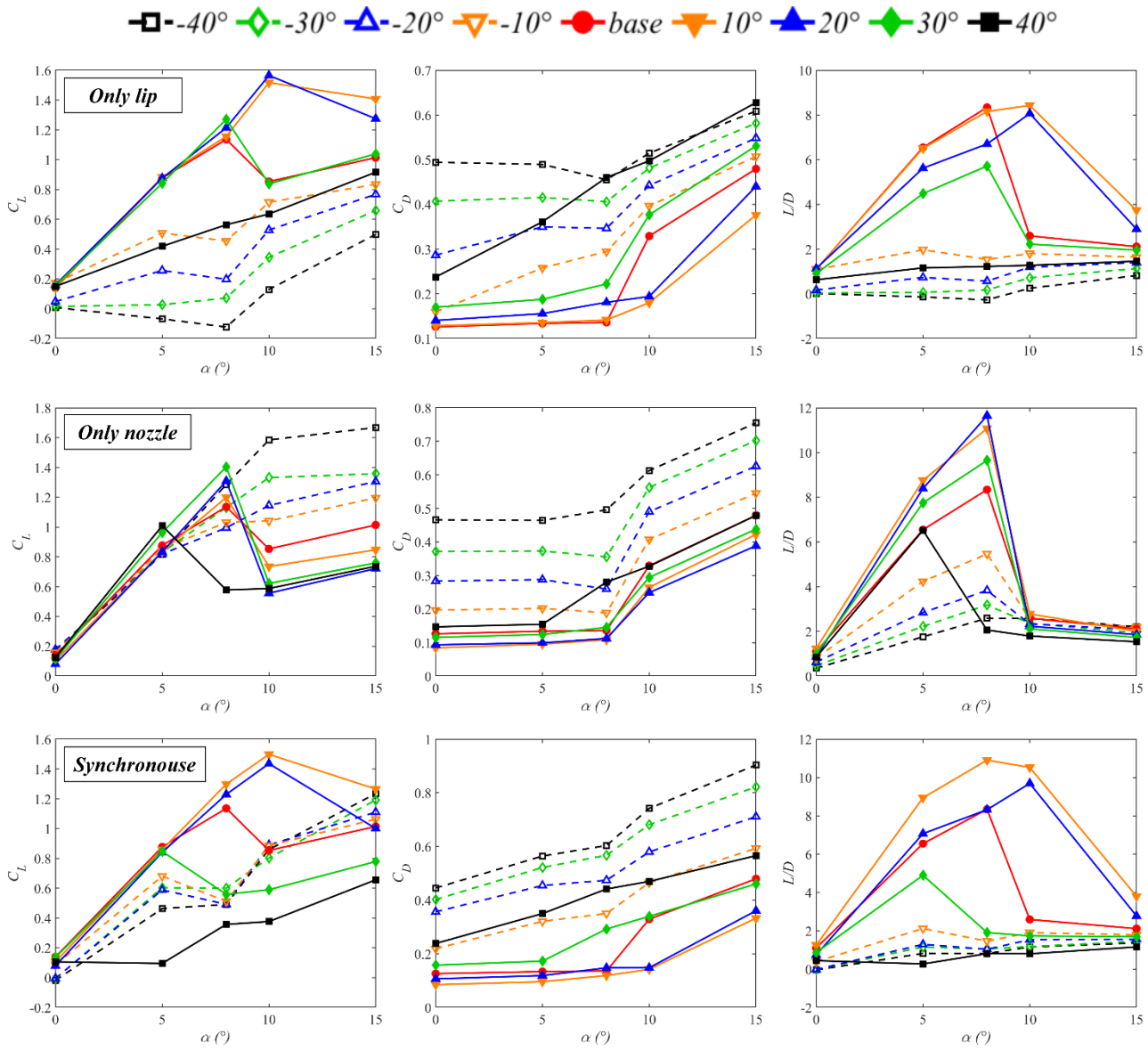
First, the curves of duct wall aerodynamic characteristics versus deflection angle at zero angle of attack for the four configurations are presented. It can be observed that:

(1) The “Opposite” configuration exhibits the highest overall drag coefficient, and its curve is roughly symmetric. The drag reaches a minimum at a deflection angle of –10°. As the absolute deflection angle increases in both positive and negative directions, flow separation intensifies and drag increases rapidly. The other three configurations show similar drag trends: as the deflection angle increases from negative to 10°, drag continuously decreases, and each configuration achieves minimum drag at a contraction angle of 10°. Further increasing the contraction angle causes drag to rise again. Notably, the minimum drag state of the “Opposite” configuration also corresponds to nozzle contraction, but due to simultaneous lip expansion, its drag coefficient is still slightly higher than that of the “Only nozzle” configuration contracted only by 10°. Moreover, simultaneous contraction of lip and nozzle by 10° does not yield lower drag. This indicates that, under internal-external flow coupling, contracting only the nozzle by a certain angle is the most effective and simple drag reduction strategy.

(2) The propulsion wing unit can be analogously considered as a biplane configuration. When the absolute deflection angle increases, the camber of the upper and lower duct walls changes in opposite directions (one increases while the other decreases). Therefore, even under contraction deformation, lift gain may still occur. From the lift coefficient curves, it can be seen that in the positive deflection angle range, the lift of the “Only lip” and “Opposite” configurations is slightly higher than the baseline within 30°, while the “Only nozzle” and “Synchronous” configurations remain below the baseline and

exhibit adverse effects after 20°, which is related to the asymmetric evolution of flow separation characteristics caused by the change in wall camber. In the negative deflection angle range, the “Only lip” and “Opposite” configurations show significant lift enhancement at small deformation angles, with the “Opposite” configuration achieving the best lift characteristics at –10°. However, as the deflection angle further increases, both configurations experience pronounced flow separation, and lift drops rapidly. The lift enhancement capability of the “Only nozzle” configuration persists up to –20°, but its maximum lift coefficient is not superior to that of the “Only lip” configuration. Overall, moderate lip expansion is a simple and effective means of increasing lift, and simultaneous moderate nozzle contraction can further improve lift characteristics.

Overall, under zero angle of attack, fixed freestream velocity, and fixed rotational speed, the single nozzle contraction scheme offers a significant drag reduction effect within a deflection angle of 10°. Although lift decreases, the overall lift-to-drag ratio improves. When moderate lip expansion is further introduced, the “Opposite” configuration at a deflection angle of –10° achieves drag approximately equal to the baseline while lift increases by more than 40%, resulting in a lift-to-drag ratio significantly superior to the other three configurations. This demonstrates excellent performance in lift enhancement and efficiency improvement.



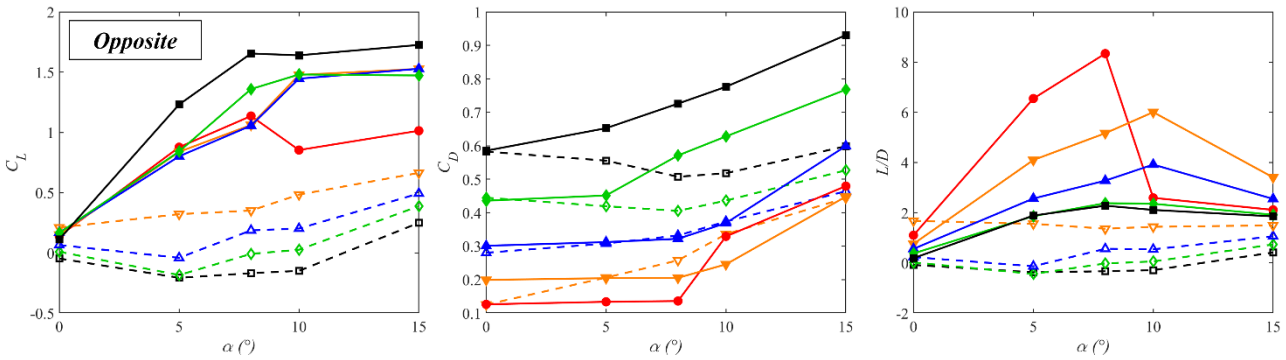


Figure 11 – Aerodynamic characteristic curves of different configurations versus angle of attack ($N = 7000r/min, V = 30m/s$).

Figure 11 further presents the variation of aerodynamic characteristics with angle of attack for the four configurations. Different line types and symbols correspond to different deflection angles. It can be observed that:

(1) Consistent with conventional wings, the drag coefficient of each configuration increases with angle of attack. Furthermore, larger absolute deflection angles lead to higher drag coefficients at zero angle of attack and higher growth rates. The “Only lip” configuration exhibits the largest wetted area at a deflection angle of -40°, and consequently the highest drag throughout the range. At +40°, its drag increases most rapidly, possibly due to strong flow separation on the inner wall induced by excessive lip contraction. Beyond an angle of attack of 8°, the configurations with lip contraction of 10° and 20° show significantly lower drag than the baseline, and the abrupt drag rise is delayed until after 10°, indicating that moderate lip contraction can effectively postpone flow separation. For the “Only nozzle” configuration, drag increases gently before 8° angle of attack, and the overall drag at each deflection angle is slightly lower than that of “Only lip”. As the angle of attack further increases, drag grows rapidly. In the negative deflection range, both the drag increment and the maximum drag are higher than those of “Only lip”; in the positive deflection range, the growth is relatively milder, and drag remains below the baseline when the nozzle deflection angle is less than 40°. The “Synchronous” configuration combines the advantages of the previous two in the positive deflection range. Especially at high angles of attack, when the synchronous contraction angle does not exceed 20°, its drag is further reduced compared with the other two schemes, demonstrating superior drag reduction capability. The “Opposite” configuration exhibits the highest drag among the four schemes, with drag increasing monotonically with angle of attack. Its additional drag penalty is significant across the entire angle-of-attack range; even with positive deflection, its drag remains considerably higher than that of the other configurations.

(2) Both deflection angle and configuration influence the nonlinear lift response, causing significant differences in peak lift and stall angle. Compared with the baseline, the “Only lip” configuration suffers severe lift loss when the lip expands, worsening with larger expansion angle. When the lip contracts, lift improves: below 5°, lift is similar to baseline; at 8°, lift rises substantially. For contraction angles $\leqslant$ 20°, the stall angle delays to 10°, matching the drag curve inflection point, further confirming the positive effect of lip contraction. However, excessive contraction decrease the stall angle; at 40°, lift enhancement vanishes. The “Only nozzle” configuration behaves differently. With nozzle contraction (positive deflection), the lift curve shifts upward but lift loss increases after 8°. When contraction reaches 40°, stall angle decreases to 5°. With nozzle expansion (negative deflection), lift improves: as expansion angle grows, the lift curve approaches the baseline before 8°, and stall angle progressively delays. At 40° expansion, lift coefficient rises up to 15° angle of attack, reaching nearly 1.7. For the “Synchronous” configuration compared to “Only lip”: simultaneous lip/nozzle expansion yields weak lift; simultaneous contraction $\leqslant$20° gives clear lift enhancement and stall delay. However, due to lift loss from nozzle contraction, “Synchronous” has slightly lower lift enhancement than “Only lip”. The “Opposite” configuration combines features of both “Only lip” and “Only nozzle”. At negative deflection (lip expansion, nozzle contraction), lift characteristics are worst. At positive deflection (lip contraction, nozzle expansion), lift is highest. Although stall angle does not improve, lift coefficient generally continues rising with angle of attack, with particularly strong lift enhancement at medium and high angles.

In terms of lift-drag performance, the “Only lip” configuration achieves its optimal efficiency range at

8°–10° angle of attack, with the best overall performance at a lip contraction of 10°, but its maximum lift-to-drag ratio is only about 8. The “Only nozzle” configuration peaks at 8° angle of attack. Although nozzle expansion gives excellent lift characteristics, it also incurs the largest drag increase, resulting in the best lift-to-drag ratio instead at 20° nozzle contraction. The “Opposite” configuration is also constrained by high drag, with a generally low lift-to-drag ratio—even lower than the baseline at low to medium angles of attack—limiting its overall performance under all deflection conditions. The “Synchronous” configuration achieves a good balance between lift and drag. With simultaneous lip and nozzle contraction of 10°, it has the best lift-to-drag ratio across the entire angle-of-attack range, reaching a maximum of about 11, which represents a nearly 35% improvement over the baseline.

4.3 Flow field characteristics

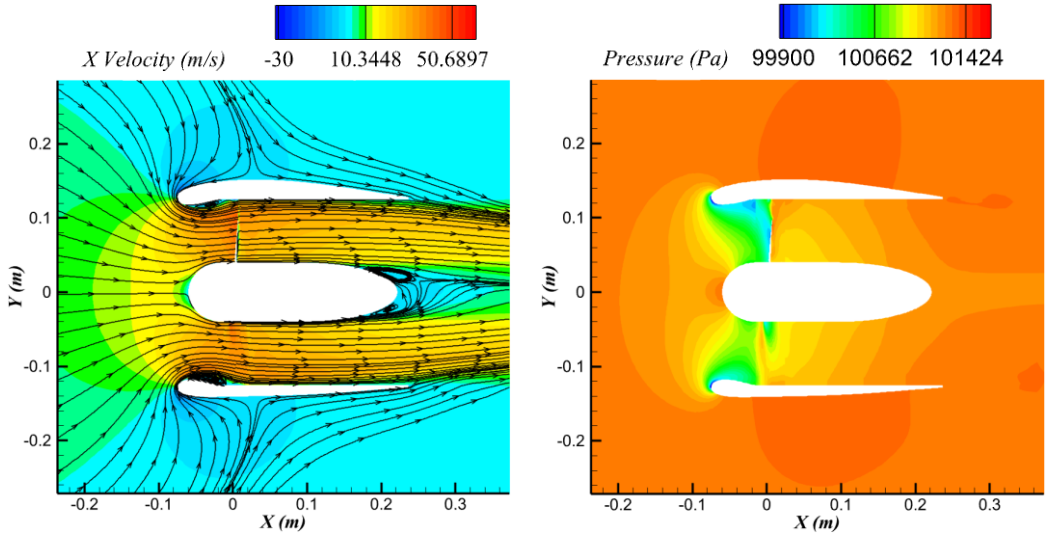
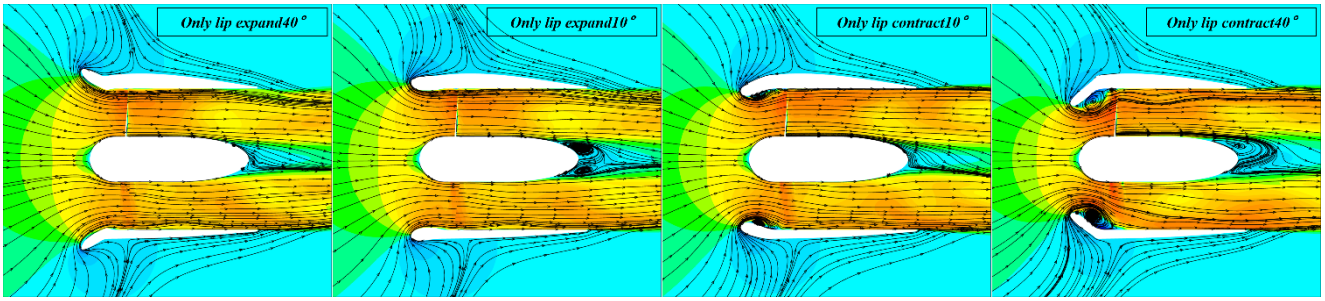


Figure 12 – Velocity and pressure contours of the flow field for the baseline configuration under hovering condition ($N = 7000r/min, V = 0m/s$).

Figure 12 first presents the flow field characteristics and flow structure on the central cross section of the baseline configuration under hovering condition. It can be observed that, under hovering, the suction effect of the propulsion wing unit is very significant: a large volume of air upstream of the lip is accelerated into the duct by suction, forming strong suction peaks at both the upper and lower lip leading edges, and correspondingly generating a strong low-pressure region ahead of the rotor disk, thereby providing substantial thrust to the duct. However, due to the thin lip, the accelerated airflow cannot fully follow the highly curved leading edge, resulting in small local separation vortices near the inner wall leading edges of both lips. In addition, influenced by the hub shape, the swirling rotor jet induces flow separation in its wake. Under the combined effect of these two phenomena, a certain amount of thrust loss occurs.



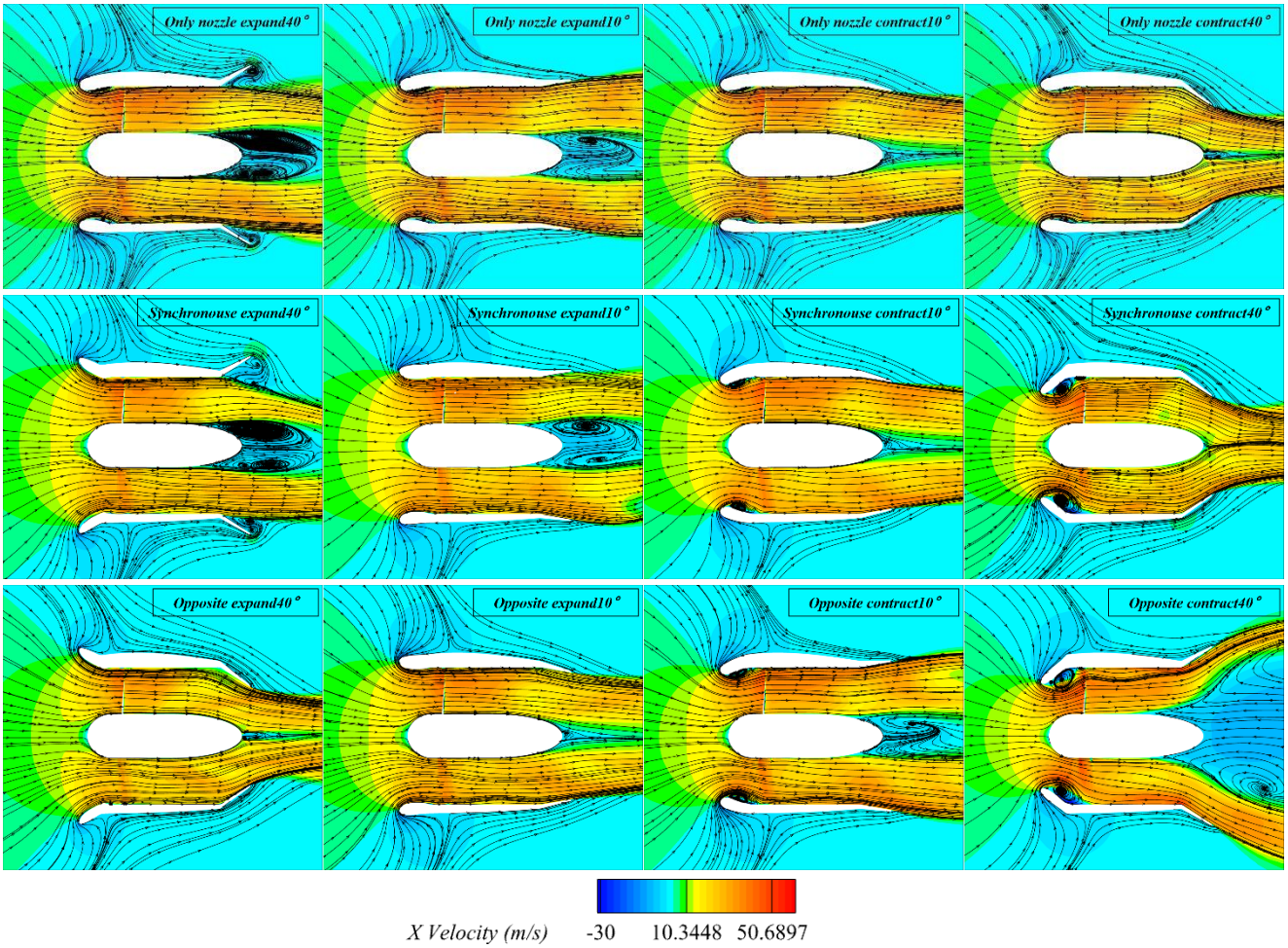


Figure 13 – Comparison of Velocity Streamline Contours for Different Configurations ($N = 7000r/min, V = 0m/s$).

Figure 13 further presents the velocity streamline contours of the four configurations under hovering condition at absolute deflection angles of 10° and 40°. It can be observed that:

(1) For the “Only lip” configuration, after lip expansion, although the flow separation in the hub wake is not significantly improved, the local separation vortex near the inner wall leading edge disappears, inlet distortion reduces, and duct wall thrust increases. However, duct suction weakens, rotor disk inflow velocity drops slightly, and the mass flow through the rotor disk is reduced, leading to rotor thrust loss. As expansion angle increases further, suction coverage expands slightly, total mass flow recovers, and rotor thrust increases a bit—though still below baseline, with lower power consumption. Consequently, total thrust rises slightly with expansion angle, while thrust efficiency stays above baseline. When lip contracts, the lip leading edge separation vortex grows, inlet flow quality worsens, leading to a quick drop in duct wall thrust. But duct suction strengthens; despite distortion losses, rotor inflow velocity rises significantly, increasing mass flow and rotor thrust with contraction angle, along with power consumption. As seen in Figure 8, rotor thrust gain cannot offset duct thrust loss from separation, leading to a rapid drop in thrust efficiency.

(2) For “Only nozzle”, as the nozzle expands, the velocity distribution around the rotor disk remains largely unchanged, but the jet velocity decreases and the separation vortex in the hub wake intensifies significantly, causing a clear duct thrust loss that keeps it below baseline. Notably, when the expansion angle becomes sufficiently large, the jet is no longer constrained by the nozzle shape and naturally contracts behind the rotation point, halting further duct thrust drop. Additionally, two high pressure separation vortices form at the upper and lower nozzle trailing edges, slightly recovering duct thrust, though it remains below baseline. When the nozzle contracts, the jet velocity increases slightly, the hub wake separation vortex is suppressed, and duct thrust rises. However, as the contraction angle further increases, the effective nozzle exit area shrinks substantially, leading to local choking near the nozzle. The jet then develops unevenly, local velocity drops significantly, reducing the effective jet flow and causing notable duct wall thrust loss. This explains the duct wall thrust trend in Figure 8. For the rotor, flow choking raises the pressure behind rotor disk, increasing rotor thrust,

which compensates for the duct thrust loss and ensures total thrust increases.

(3) The “Synchronous” configuration combines flow features of the previous two. With synchronous expansion, lip expansion improves inflow similar to “Only lip”, and the higher-quality inflow weakens the hub wake separation vortex compared to “Only nozzle”, while the effect on the rotor remains close to that of “Only lip”. Consequently, both duct wall thrust and total thrust lie between the two. With synchronous contraction, the suction effect enhances rotor inflow velocity, and local jet choking at large deflection raises the pressure behind the rotor, giving this configuration the highest rotor thrust. However, on the duct wall side, it inherits the drawbacks of both previous schemes, and the thrust loss is further increased. In this case, the rotor thrust gain cannot offset the duct wall thrust loss, so total thrust still lies between the two, and thrust efficiency remains below baseline, consistent with the thrust characteristics shown in Figure 8.

(4) Within an appropriate negative deflection angle range, the “Opposite” configuration successfully combines the advantages of the two single-deformation schemes: lip expansion eliminates the separation vortex at the inner wall leading edge, while nozzle contraction suppresses the hub wake separation vortex and accelerates the jet. Consequently, both duct wall thrust and rotor thrust are enhanced, yielding higher total thrust and efficiency than the other three schemes. However, when the deflection angle increases to -40°, the combined effect of weakened suction and local jet choking causes a substantial drop in duct wall thrust, leading to reduced efficiency. Similarly, in the positive deflection range, this configuration inherits the drawbacks of both single deformation schemes: flow separation at the lip leading edge and hub wake intensifies significantly, corresponding to the marked drop in thrust and efficiency observed in Figure 8, and the propulsive performance advantage is completely lost.

Overall, under hovering condition, the internal flow state can be effectively regulated by deflecting the lip and nozzle. Single deformation schemes (e.g., contracting only the lip or only the nozzle) are simple in structure and can enhance thrust and efficiency. Appropriate combined deformation (e.g., the “Opposite” configuration at –10° deflection) can further synergistically optimize flow details such as flow attachment and jet velocity, balancing the propulsive characteristics of both duct wall and rotor, thereby achieving optimal hovering efficiency.

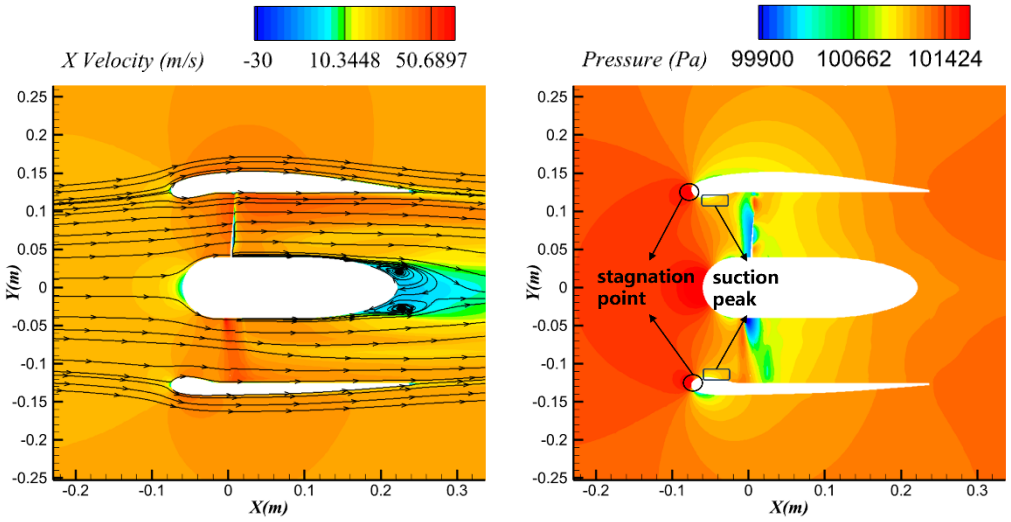


Figure 14 – Velocity and pressure contours of the flow field for the baseline configuration under cruising condition ($N = 7000r/min, V = 30m/s$).

Figure 14 shows the flow field and structure of the baseline configuration under cruising condition at the same rotational speed. Under high-speed freestream, the internal and external flows are highly coupled. The duct wall behaves like a biplane, with dual stagnation points and dual suction peaks: external flow corresponds to stagnation points, internal flow to suction peaks. Compared with hovering (Figure 12), duct suction is much weaker, but inner wall velocity remains higher than outer wall. Moreover, the inner wall leading edge flow stays attached without separation, and the hub wake recirculation zone is significantly reduced. However, the low-pressure region ahead of the rotor disk is greatly diminished, and a large high-pressure region appears in front of the lip due to stagnation, causing a sharp drop in overall thrust.

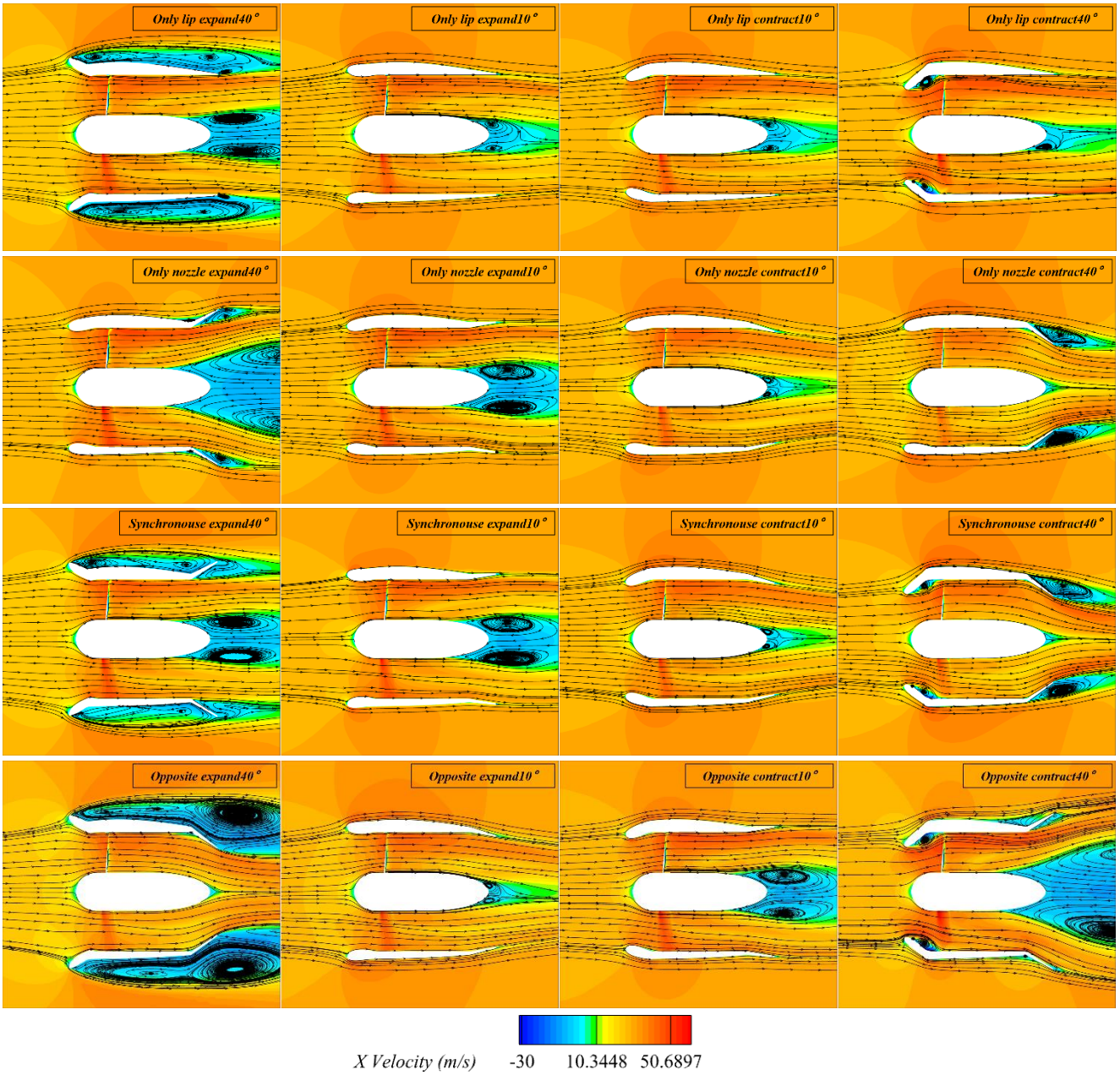


Figure 15 – Comparison of Velocity Streamline Contours for Different Configurations ($N = 7000r/min, V = 30m/s$).

Figure 15 presents axial velocity contours and streamline distributions of the four configurations under cruising condition, providing flow mechanism support for the aforementioned conclusions on aerodynamic-propulsion coupling characteristics. It can be observed that:

(1) For the “Only lip” configuration, the internal flow variation with lip expansion under cruising condition is similar to that under hovering: the duct inlet area increases, the suction effect weakens, the velocity ahead of the rotor disk drops slightly, leading to reduced rotor thrust. Meanwhile, the duct wall is significantly affected by the external flow: expansion increases the wetted area, the stagnation zone at the leading edge expands, duct wall drag rises, which manifests as thrust loss. Notably, lip expansion causes opposite camber changes on the upper and lower walls (upper wall effective camber decreases while lower wall camber increases) resulting in lift enhancement. However, as the expansion angle further increases, the high-speed external flow forms strong flow separation around the outer lip, generating large low-speed recirculation zones on both upper and lower outer duct walls, causing a sharp rise in wall drag and a substantial drop in lift. The separation spreads to the duct trailing edge, intensifying jet energy dissipation and hub wake separation, thereby severely deteriorating duct thrust and rapidly reducing overall propulsive performance.

When the lip contracts, the duct inlet area decreases. The high-speed freestream is compressed into the duct, increasing the flow velocity near the lip, improving inlet flow quality, and expanding the

high-speed region. Both duct wall and rotor thrust increase, and separation at the hub trailing edge is suppressed, with drag lower than under expansion. However, as the contraction angle further increases, the high-speed external flow forms a strong bypass on the inner side of the lip, inducing local separation vortices at the inner wall leading edge and deteriorating the wall pressure distribution, leading to lift and thrust degradation.

(2) For the “Only nozzle”, nozzle expansion increases the duct exit area, slightly reduces jet velocity, and intensifies flow separation at the hub trailing edge. Meanwhile, the high speed jet near the nozzle trailing edge no longer develops along the wall, causing a drop in inner wall velocity downstream. Under the high speed external flow, a small recirculation zone forms at the trailing edge, further increasing duct thrust loss. Regarding lift characteristics, this configuration resembles “Only lip”, but due to weakened flow attachment from trailing edge expansion, the lift increase is smaller. When the nozzle expands to 40°, similar to hovering: hub trailing edge separation worsens, and a recirculation zone appears on the inner wall at the nozzle trailing edge, but constrained by the high speed external flow, this separation does not spread to the outer wall. Multiple flow losses accumulate, causing duct thrust loss. Additionally, the greatly expanded nozzle structure induces slight separation at the deflection corner, increasing aerodynamic drag. Notably, the flow separation in this configuration is mainly induced by internal flow, with little effect on the outer wall aerodynamic state; thus overall duct lift does not degrade significantly. Moreover, the effective camber increases slightly, yielding a modest lift increase over the baseline.

When the nozzle contracts, the internal flow variation is consistent with hovering: at small contraction angles, the jet accelerates, the hub wake separation vortex is suppressed, both duct wall and rotor thrust increase; at large angles, jet choking occurs, the rotor thrust gain compensates for duct wall thrust loss, improving overall propulsive performance. In addition, the high-speed regions on both upper and lower outer walls gradually expand, but the increase on the lower wall is greater than on the upper wall, reducing the wall pressure difference and thereby decreasing lift. However, as the contraction angle further increases, significant flow separation appears on both outer walls at the nozzle, with stronger separation on the upper wall than on the lower wall, which slightly recovers lift, though overall lift remains below baseline.

(3) The “Synchronous” configuration also combines the flow features of lip and nozzle deflection, and its flow field is jointly affected by the structural changes of both. With synchronous expansion, flow separation easily occurs around the outer lip, reducing inlet flow uniformity; a large recirculation vortex forms at the nozzle tail, increasing exit flow losses. The dual separation effects superimpose, significantly degrading wall flow attachment, causing a sharp rise in duct drag and a continuous drop in lift. With synchronous contraction, the flow field of the “Synchronous” configuration closely resembles that of “Only nozzle”, so their propulsive and aerodynamic characteristics are generally similar. However, as the contraction angle increases, a separation vortex gradually appears at the lip leading edge, leading to performance deterioration of this configuration.

(4) Under negative deflection angles, the lift variation trend of the “Opposite” configuration is consistent with “Only lip”, further indicating that lip deflection has a stronger effect on adjusting the effective camber of the airfoil than nozzle deflection. Meanwhile, the jet acceleration due to nozzle contraction further enhances the lift increase, making the “Opposite” configuration achieve the best lift at -10° deflection. Moreover, the thrust increase from nozzle contraction compensates for the drag increase caused by lip expansion, giving this configuration the highest lift to drag ratio. However, as the deflection angle continues to increase, flow separation induced by lip flow around and excessive nozzle contraction superimpose, forming a large separation zone on the outer duct wall, resulting in the worst lift characteristics instead.

When the deflection combination switches to lip contraction and nozzle expansion, a good flow state can still be maintained at small angles, with only increased flow separation at the hub trailing edge and a slight loss in propulsive performance. In this case, both upper and lower airfoils exhibit an S like shape. The trailing edge upturn reduces the high speed (low pressure) regions on both outer walls, especially on the lower wall. Under the combined effect, lift increases slightly instead. At large deflection angles, the adverse flow effects of both “Only lip” and “Only nozzle” configurations superimpose: flow separation behind the hub and at the nozzle outer wall inflection point worsens further, leading to a significant degradation in both aerodynamic and propulsive performance.

Overall, under both hovering and cruising conditions, deflecting the lip and nozzle can effectively regulate the flow state. Single-deformation schemes (such as contracting only the lip or only the nozzle) are structurally simple and can enhance thrust or lift under their respective operating conditions, but the performance improvement is limited. Appropriate combined deformation (e.g., the

"Opposite" configuration at -10° deflection) can further synergistically optimize flow details such as flow attachment, jet velocity, and airfoil camber, balancing the propulsive characteristics of both duct wall and rotor while achieving the best lift-to-drag ratio and hovering efficiency. However, under either hovering or cruising, excessive deflection angles will induce superposition of multiple flow separations, leading to significant degradation of aerodynamic and propulsive performance. Therefore, selecting a suitable deflection combination and angle is key to achieving efficient operation of the propulsion wing unit over a wide range of conditions.

4.4 Wall pressure distribution

As shown in Section 4.2, when an angle of attack is present, each configuration achieves a relatively favorable lift-to-drag ratio at a deflection angle of 10°. Therefore, this section analyzes the wall pressure distribution at this deflection angle. The figure below presents the pressure coefficient distribution curves on the upper and lower duct walls for each configuration at different angles of attack, providing direct insight into how the deflected configurations regulate the wall pressure distribution and lift characteristics.

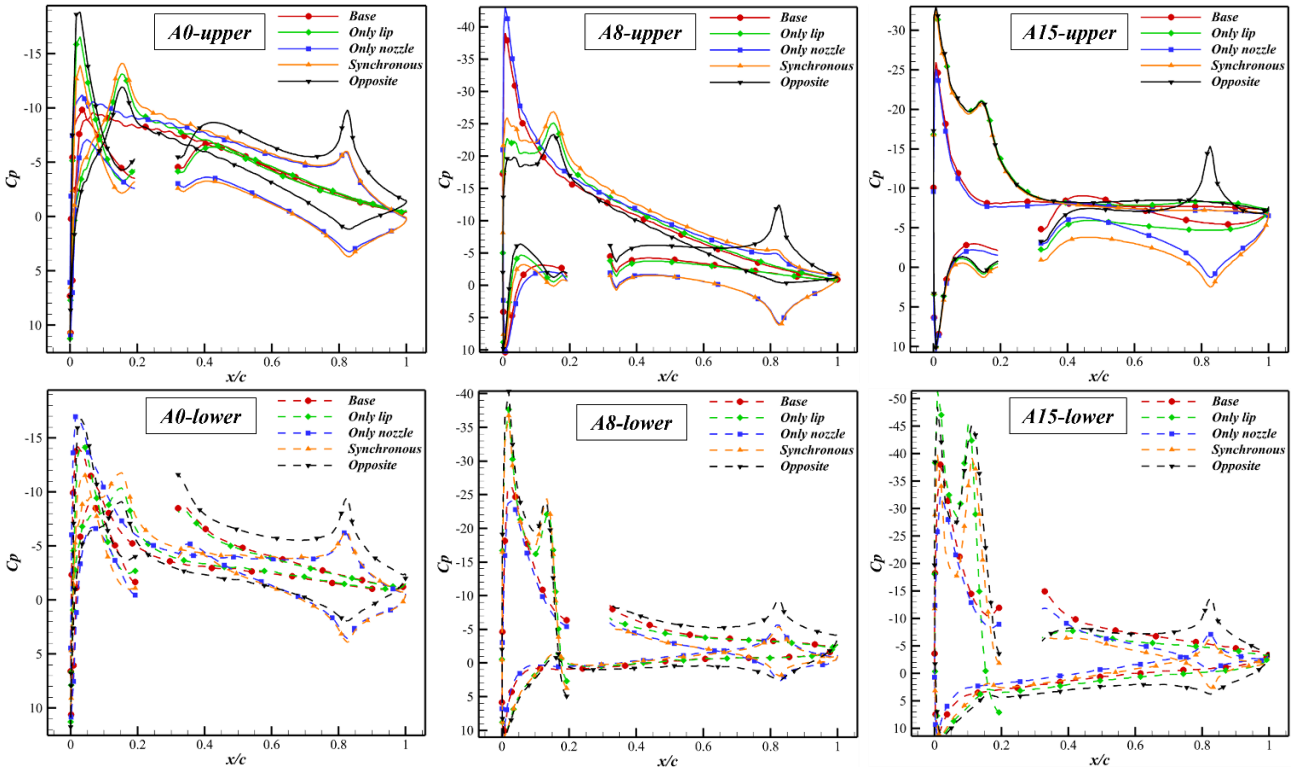


Figure 16 – Upper and lower duct wall pressure distributions for various configurations at different angles of attack ($N = 7000r/min, V = 30m/s$).

It can be observed that: (1) When $\alpha = 0°$, the incoming flow is symmetric and uniform. For the baseline configuration, the flow field and pressure distribution on the upper and lower duct walls exhibit good symmetry: the leading edge is a high-pressure stagnation point, and a low-pressure suction peak forms at the inner wall leading edge. Downstream of the rotor disk, the pressure on both inner and outer walls transitions smoothly, the pressure recovery at trailing edge is sufficient, and there is no significant internal flow separation, providing the duct with a baseline lift. For the "Only lip", the pressure distribution downstream of the rotor disk essentially coincides with that of the baseline, but lip deflection significantly alters the pressure evolution upstream of the rotor disk. Lip contraction enhances the suction effect, substantially increasing the suction peak at the inner wall leading edge. The external flow, forced to squeeze and converge at the lip front, rapidly attaches along the contracted outer wall profile, resulting in a sharp local velocity increase and forming a strong low-pressure region at the lip deflection point. The intensified suction peak increases the negative pressure difference between the inner and outer walls, causing lift loss; meanwhile, the accelerated flow around the outer wall increases the pressure difference between the outer and inner walls, generating lift gain. Under the combined effect of these two factors, the lift increase of the "Only lip"

configuration is rather limited.
The pressure differences of the “Only nozzle” configuration are mainly concentrated in the nozzle region. Nozzle contraction reduces the effective flow passage area and increases the mainstream velocity. However, the near-wall boundary layer fluid is constrained by the wall deflection, which hinders its acceleration and prevents it from being expelled synchronously with the mainstream. As a result, the static pressure on the inner wall downstream of the rotor disk is significantly higher than that of the baseline configuration, gradually transitioning to the ambient pressure at the exit only after passing the inner wall deflection point. Meanwhile, nozzle contraction changes the camber of the airfoil tail, creating a curvature discontinuity at the outer wall deflection point. The upstream parallel flow is forced to contract and turn at this point, causing local over-acceleration and thus forming a distinct negative pressure peak on the outer wall, which increases the pressure difference on the upper wall. A similar trend occurs on the lower wall: both the negative pressure on the outer wall and the positive pressure on the inner wall increase, resulting in lift loss on the lower wall. Under the combined effect, the effective pressure difference across the duct decreases, ultimately causing a reduction in the lift coefficient compared with the baseline configuration.
The “Synchronous” configuration clearly inherits the dual flow characteristics of both “Only lip” and “Only nozzle” in terms of wall pressure coefficient distribution: the leading-edge pressure distribution is highly similar to that of “Only lip”, while the pressure distribution in the nozzle region essentially coincides with that of “Only nozzle”. Therefore, its overall lift characteristics are largely consistent with those of “Only lip”.
For “Opposite”, leading-edge pressure distribution matches “Only lip”. Due to opposite nozzle deflection, its nozzle region pressure distribution is opposite to “Only nozzle”. Inner wall pressure coefficient downstream of rotor disk drops significantly, indicating nozzle expansion’s deceleration is much weaker than lip contraction’s suction acceleration, thus overall internal flow accelerates. On outer wall, lip contraction accelerates leading-edge external flow, but nozzle expansion and upturn reduce outer wall velocity downstream of rotor disk, increasing pressure coefficient. This coupling reduces upper wall lift; however, lower wall gains lift from both internal and external flow changes, and the lower wall gain outweighs upper wall loss, leading to overall lift increase.
(2) At non-zero angles of attack, the flow on the upper and lower duct walls becomes significantly asymmetric. As the angle of attack increases, flow field distortion and performance differentiation intensify. The baseline configuration behaves like a conventional wing: at 8° angle of attack, a strong low-pressure region appears at the leading edge of the upper outer wall, reducing the outer wall pressure; the lower wall experiences a pressure increase due to the stagnation effect. The pressure difference between the upper and lower walls is greatly enhanced compared with the 0° case, resulting in a significant lift increase. When the angle of attack increases to 15°, flow separation on the upper wall intensifies, the adverse pressure gradient at the trailing edge worsens, pressure recovery becomes impossible, and lift degrades.
The upper wall pressure distribution of “Only lip” shows a bimodal characteristic: after the stagnation point, flow accelerates to form the first low-pressure peak. At 10° contraction, the local angle of attack in the rotated lip section decreases, flow becomes smooth, and pressure recovery slows. Passing the deflection point, curvature discontinuity causes re-acceleration, forming a secondary peak. Compared with baseline, peak values are lower but negative pressure area expands, giving a larger pressure difference. The lower inner wall also shows two peaks: after the leading-edge suction peak, the deflected section separates at non-zero angles of attack, pressure recovers, then flow reattaches and accelerates at the deflection point, creating a secondary peak. On the outer wall, lip contraction shifts the stagnation point rearward, enlarging the leading-edge high-pressure region, which further increases the lower wall pressure difference. At high angle of attack, inner wall separation occurs earlier and intensifies, causing some lift loss. Nevertheless, overall lift remains above baseline, showing good stability over a wide angle-of-attack range.
For “Only nozzle”, pressure distribution upstream of the rotor disk matches the baseline, with differences at the trailing edge and inner wall. At 8° angle of attack, upper inner wall pressure increase and outer wall negative protrusion still exist, but a trailing-edge recirculation zone raises negative pressure, slightly reducing lift gain. On the lower wall, similar to baseline, outer wall pressure increases, and both leading-edge suction peak and inner wall negative pressure are enhanced, producing lift increase. Overall, lift is slightly above baseline. As angle of attack increases, upper outer wall separation intensifies, the local acceleration at the deflection point disappears, and upper wall lift gain becomes more limited. Meanwhile, lower wall jet choking occurs, and pressure recovery at the inner trailing edge causes additional lift loss. Therefore, the lift of the “Only nozzle” configuration

degrades at high angles of attack.

The “Synchronous” configuration consistently inherits the leading-edge characteristics of “Only lip” and the trailing-edge characteristics of “Only nozzle”. At low angle of attack, its synchronous contraction integrates the lift enhancement features of the single-deformation schemes, achieving the best lift performance. At high angles of attack, although flow separation still occurs, the lift gain advantage of lip contraction is sufficient to compensate for the loss caused by nozzle contraction, allowing this configuration to maintain a relatively high lift level.

The “Opposite” configuration exhibits a distinct advantage in high-angle-of-attack adaptability. While inheriting the wide-angle lift enhancement capability of the “Only lip”, it effectively suppresses flow separation at the nozzle on the upper outer wall at high angle of attack by means of nozzle expansion, thereby maintaining the upper wall pressure difference. Meanwhile, the features of lower outer wall pressure increase and inner wall negative pressure peak, which are further strengthened by the expansion and upturn of the nozzle, enhance the pressure difference gain on the lower wall. As a result, this configuration can still increase lift at high angles of attack, demonstrating excellent aerodynamic regulation capability at high angles of attack.

In summary, the core flow control mechanisms are geometry-induced local acceleration and deceleration and separation suppression. Lip contraction reduces the local angle of attack at the inlet and, combined with curvature discontinuity, creates a double-peak negative pressure region, expanding the low-pressure coverage. Nozzle contraction accelerates the mainstream, but at large angles it tends to cause jet choking, leading to lift loss. Nozzle expansion suppresses upper wall separation but comes with energy loss due to mainstream deceleration. Through coordinated design of deflection schemes and angles (e.g., the “Synchronous” configuration integrating leading-edge and trailing-edge advantages, and the “Opposite” configuration using expansion and upturn to enhance lower wall pressure difference and suppress upper wall separation), the wall pressure distribution and boundary layer state can be effectively regulated. This achieves a balance between pressure difference gain and separation control at different angles of attack, thereby obtaining wide-angle aerodynamic optimization capability.

5. Conclusion

This paper takes the propulsion wing unit as the research object to address the difficulty of achieving high efficiency for fixed-geometry ducted fans under a wide range of operating conditions (hover and cruise). Systematic numerical simulations and mechanism analyses are carried out. First, a parametric model that allows independent or coordinated deflection of the lip and nozzle is established, enabling automatic generation of complex curved surfaces. Then, based on CFD methods, the propulsive and aerodynamic characteristics of four deformation schemes are comparatively studied under different freestream velocities, rotational speeds, and angles of attack. The flow field evolution and wall pressure regulation mechanisms under varying key geometric parameters are revealed. The main conclusions are as follows:

(1) Single lip or nozzle deflection improves hover and cruise performance but shows strong operating-condition dependence. Under hovering, internal flow dominates: lip deflection improves inflow, eliminates leading-edge separation, enhances duct wall thrust, and boosts efficiency. Under cruising, external flow dominates: lip expansion increases wetted area and drag sharply, while lip contraction gives little thrust gain. In contrast, nozzle deflection increases thrust via jet acceleration and trailing-edge separation suppression, improving cruise efficiency. single-deformation schemes should be matched to the operating condition: lip expansion is recommended for hovering, while nozzle contraction is recommended for cruising.

(2) Coupled lip and nozzle deflection, under an appropriate combination scheme, can fully inherit the flow control advantages of both lip and nozzle, enabling further performance breakthrough, achieving both hovering thrust efficiency and cruising efficiency, and significantly expanding the usable angle-of-attack range. With synchronous small-angle contraction of lip and nozzle, both leading-edge diffusion and jet acceleration are achieved, yielding an optimal lift-to-drag ratio that is nearly 35% higher than the baseline. Under hovering and small angles of attack, opposite deflection of lip and nozzle (lip expansion combined with nozzle contraction) can eliminate leading-edge separation via lip expansion and suppress trailing-edge recirculation via nozzle contraction, achieving optimal thrust and thrust efficiency. However, when the deflection angle becomes too large, coupled schemes often lead to superposition of multiple flow separations, causing rapid performance deterioration.

(3) The core flow mechanism by which lip/nozzle deflection improves aerodynamic performance is

geometry-induced local acceleration/deceleration and separation suppression. Lip contraction reduces the effective local angle of attack at the upper wall inlet, combined with curvature discontinuity, creates a double-peak negative pressure region, expanding the low-pressure coverage and delaying stall. Nozzle contraction accelerates the mainstream and suppresses trailing-edge separation, but at large angles it tends to induce jet choking, leading to lift-to-drag ratio loss. Nozzle expansion suppresses upper wall separation and strengthens lower wall pressure, but the mainstream deceleration often incurs energy loss. Through coordinated design of lip and nozzle deflection angles, the wall pressure gradient and boundary layer attachment state can be more effectively regulated, achieving a balance between pressure difference gain and separation loss under different operating conditions.

In summary, rationally matching the deflection mode and angle range of the lip and nozzle can effectively regulate the internal-external flow coupling characteristics and wall pressure distribution of the propulsion wing unit, suppress flow separation distortion over a wide range of operating conditions, and balance hovering propulsion efficiency with cruising aerodynamic performance. These results provide theoretical basis and technical reference for configuration optimization, wide-condition propulsion/aerodynamic integrated design, and flow control mechanism analysis of the propulsion wing unit.

6. Acknowledge

This work was supported by National Natural Science Foundation of China (12502386).

7. Contact Author Email Address

Minghao Li: liminghao964@mail.nwpu.edu.cn

Zhou Zhou: zhouzhou@nwpu.edu.cn

Kelei Wang: craig-wang@nwpu.edu.cn

8. Copyright Statement

The authors confirm that they, and/or their company or organization, hold copyright on all of the original material included in this paper. The authors also confirm that they have obtained permission, from the copyright holder of any third party material included in this paper, to publish it as part of their paper. The authors confirm that they give permission, or have obtained permission from the copyright holder of this paper, for the publication and distribution of this paper as part of the ICAS proceedings or as individual off-prints from the proceedings.

References

[1] Guo Y. Development of green aviation manufacturing industry issued. China Industry News, 2023-10-27(005). http://www.scio.gov.cn/live/2023/32811/wjzc/202310/t20231019_775179.html

[2] Wei ZP, Liu F, Yang S. Development status and technical key points of VTOL fixed-wing UAV. Aircraft Design, Vol. 44, No. 1, pp 5-13, 2024.

[3] Li XH, Guo Z, Liu ZW, et al. Effect of ducted fan shape parameters on aerodynamic characteristics. Journal of National University of Defense Technology, No. 4, pp 28-33, 2016.

[4] Xiang CL, et al. A high-efficiency duct with variable lip and diffuser[P]. China Patent, CN101973391B, Aug. 8, 2012.

[5] Xagon Solutions[EB/OL]. https://xagonsolutions.com.

[6] Liu YT. A variable outlet ducted system[P]. China Patent, CN114180032A, Mar. 15, 2022.

[7] Lilium[EB/OL]. https://lilium.com.

[8] Zhao QF, Zhou Z, Li MH, etc. Propulsion-Aerodynamic Coupling Model of Distributed Powered Wing-Induced Surface. Acta Aeronautica et Astronautica Sinica, Vol. 45, No. 10, pp 129252, 2024.

[9] Wang KL, Zhou Z, Guo JH, etx. Distributed powered wing propulsion/aerodynamic coupling characteristics in forward flight condition. Acta Aeronautica et Astronautica Sinica, Vol. 45, No. 2, pp 132-150, 2024.

[10] Wang KL, Zhou Z, Li MH. Research and experimental verification of loosely coupled design method for propulsion wing unit. Acta Aeronautica et Astronautica Sinica, Vol. 46, No. 9, pp 212, 2025.

[11] Menter F R. Two-equation eddy-viscosity turbulence models for engineering applications. AIAA Journal, Vol. 32, No. 8, pp 1598-1605, 1994.

[12] Xu D, Xu XP, Xia JY, et al. Aerodynamic-propulsion coupling characteristics of distributed electric propulsion

system. Journal of Aerospace Power, Vol.39, No.9, pp 188-203, 2024.

[13] Chen GQ, Bai P, Zhan HL, et al. Research on slipstream effect of a pusher propeller UAV. Acta Aerodynamica Sinica, Vol.33, No.4, pp 554-562, 2015.

[14] QI M, WANG Z X, ZHOU L, et al. Numerical study on effects of lip geometric parameters on performance of nacelle inlet J. Journal of Propulsion Technology, Vol. 41, No. 9, pp 2021-2030,2020.

[15] Wang GC, Zhou Z, Zhao QF, et al. Analytical propulsion-Aerodynamic coupling model and validation for distributed propulsion wing lift enhancement configuration. Aerospace Science and Technology, Vol. 176, PP112012, 2026.

[16] Li MH, Zhou Z, Wang KL. Numerical/experimental study of aerodynamic/propulsive coupling performance of distributed propulsion wing. Chinese Journal of Aeronautics, 2026,104179.

[17] Xu BM, Wang KL, Zhou Z, et al. Analysis of lift–thrust coupling characteristics of wing-mounted ducted fan configurations. Acta Aeronautica et Astronautica Sinica, Vol. 47, pp 133029, 2026.